Low-Complexity Energy Detection for Spatial Modulation

Elio Faddoul, Ghassan M. Kraidy, and Ioannis Krikidis
IRIDA Research Centre for Communication Technologies
Department of Electrical and Computer Engineering, University of Cyprus
Email: {efaddo01, gkraid01, krikidis}@ucy.ac.cy

***Abstract*—In this paper, we present a non-coherent spatial modulation (SM) detection scheme appropriate for low-cost low-powered devices, where channel knowledge is restricted to the magnitude of the fading gains. We first derive a low-complexity energy detection metric for the multiple receive-antenna case based on the maximum-likelihood criterion. Next, we investigate a biased (non-negative) pulse amplitude modulation design and develop an accurate analytical framework for the symbol error rate at high signal-to-noise ratio. We compare the performance of the proposed scheme with that of the optimal/coherent maximum-likelihood receiver design. Numerical results show that the non-coherent SM outperforms the coherent SM technique for scenarios where non-negative one-dimensional constellations are employed.**

***Index Terms*—Spatial modulation, non-coherent detection receiver, energy detector, biased pulse-amplitude modulation.**

I. Introduction

Motivated by the recent growth in the number of internet-connected devices and the evolution of Internet-of-Things (IoT) applications [1], future wireless communication systems require intelligent utilization of available resources. Specifically, and due to the unparalleled increase in data traffic, new transmission technologies have been studied to minimize transceiver complexity and cost. A strong candidate that addresses this challenge is spatial modulation (SM). This technology has proven to achieve high spectral and energy efficiency while maintaining a simple design architecture in comparison to traditional multiple-input multiple-output (MIMO) and single-antenna systems [2], [3]. In addition to conventional symbol modulation, SM activates a single transmit antenna for each transmission of a constellation symbol. At the receiver side, detection is twofold; the detection of the active transmit antenna index as well as the detection of the data symbol transmitted over the activated transmit antenna. Since only one antenna is activated, a single radio-frequency (RF) chain is sufficient for transmission. Consequently, the issue of inter-channel interference and inter-antenna synchronization is completely eliminated [3], [4].

The deployment of large-scale IoT networks requires low-cost, low-power, and low-complexity devices. Accordingly, non-coherent energy detection has been exploited to meet the requirements of the IoT [5], [6]. Non-coherent systems are capable of operating without the knowledge of instantaneous channel state information (CSI). In other words, only channel magnitude estimates are available at the receiver whereas phase estimation is ignored. Inherently, this makes the system easier to implement since phase synchronization circuitry is avoided. However, this decrease in complexity comes at the cost of sub-optimal performance compared with coherent systems. Hence, a tradeoff in terms of complexity and performance is introduced. Moreover, since the receiver incorporates a form of square-law detection, i.e., energy detection, the energy levels used in the constellation must be delicately chosen in order to limit the symbol error probability. A popular constellation design consists of non-negative (biased) signaling, such as biased pulse amplitude modulation (PAM) [7]. The use of non-coherent systems with biased PAM constellations has been documented for the emerging 60-GHz millimeter-wave (mmWave) wireless personal area networks based on the ECMA-387 standard [8]. In this context, non-coherent detection has been proven to achieve a better rate-energy tradeoff than conventional coherent detection for systems with energy harvesting modules, especially when incorporating an integrated architecture of energy harvesters and information decoders for simultaneous wireless information and power transfer (SWIPT) [9], [10].

Various detection schemes corresponding to different complexity levels have been explored for SM. For instance, the maximum-likelihood (ML) detector characterizes joint detection, which searches jointly over all possible transmit antennas and constellation symbols to achieve optimal performance [11]. However, due to its high complexity, several works have tackled alternative sub-optimal schemes, by employing maximal ratio combining (MRC), sphere decoding, and signal vector-based methods, [2], [12]–[14]. Nevertheless, these solutions consider optimal and sub-optimal architectures with full receiver CSI knowledge, which in some cases cannot be perfectly obtained, especially for low-complexity devices. By making use of non-coherent reception, the authors in [15] analyze the performance of an energy detection receiver based on channel magnitude knowledge for non-negative symbol constellations. Moreover, the work in [16] considers the performance of the optimal ML detector with partial CSI knowledge for space shift-keying. In this regard, to the best of our knowledge, the use of non-coherent energy detection for SM has not been exploited to date. In this work, we investigate a scheme that combines SM techniques at the transmitter with non-coherent energy detection at the receiver. Accordingly, the main contribution of this paper

This work received funding from the European Research Council (ERC) under the European Union's Horizon 2020 research and innovation programme (Grant agreement No. 81981).

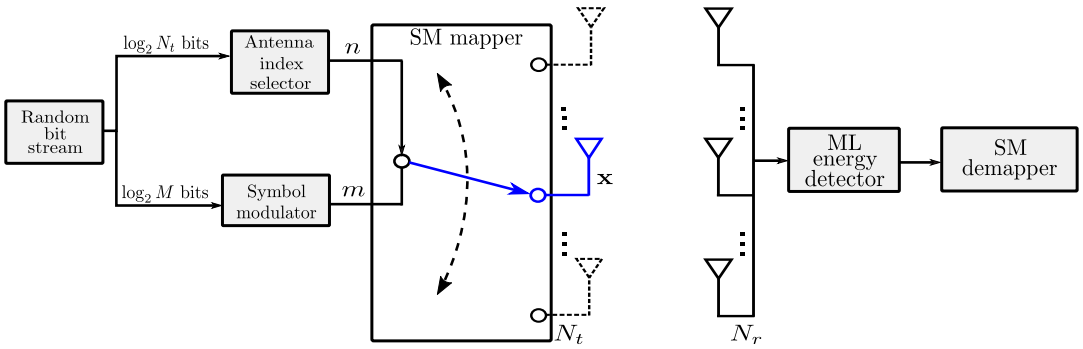

Fig. 1: Transceiver structure for non-coherent spatial modulation.

is threefold:

- We first develop a low-complexity non-coherent decision rule with multiple receive antennas for SM, based on the ML criterion, which only takes into account knowledge of the channel magnitudes and symbol energies.
- The performance of the proposed non-coherent SM scheme is then studied; a non-negative real constellation is investigated and expressions for the symbol error rate (SER) at high signal-to-noise ratios (SNRs) are derived.
- Finally, our results show that the proposed non-coherent SM detector provides a comparable performance to its coherent counterpart, whenever a non-negative constellation is used, hence making the design appropriate for low-cost low-powered devices.

The paper is organized as follows. In Section II, we present the system model for non-coherent SM based on the ML criterion. In Section III, we derive the analytical SER expressions for the non-coherent SM detector. Section IV provides the numerical results, and Section V gives the concluding remarks.

II. System Model

We consider an $N_t \times N_r$ SM system with N_t transmit antennas and N_r receive antennas, as depicted in Fig. 1. At the transmitter, the information bits are simultaneously sent over two streams; one is mapped onto the spatial constellation diagram of size N_t, whereas the other stream is mapped onto the signal constellation diagram of size M. The bit stream is divided into blocks of $\log_2(N_t M)$ bits. Each block is split into two parallel streams of $\log_2(N_t)$ and $\log_2(M)$ bits, respectively. The former stream activates one of the transmit antennas, and the latter is used to determine a symbol in the signal constellation diagram. More specifically, these $\log_2(N_t M)$ bits are mapped onto a constellation vector $\mathbf{x}$ of size N_t. In SM, only one antenna remains active during transmission, hence only one element in the constellation $\mathbf{x}$ is non-zero, which is at the position of the active antenna. As an example, given that the antenna index is used as an additional resource to transmit information, the active antenna and the symbol index constitute a mapping strategy, and the output vector is written as

$$\mathbf{x} \triangleq \begin{bmatrix} 0 & 0 & \cdots & \underset{\substack{\uparrow \\ n^{\text{th}} \text{ position}}}{s_m} & 0 & \cdots & 0 \end{bmatrix}^T,$$

where $n = 1, 2, \ldots, N_t$ represents the active antenna, and s_m is the m-th information-bearing symbol from the M-ary constellation at the n-th position.

In addition, since the receiver performs energy detection, the amplitude levels in the constellation must be asymmetric in order to avoid having two symbols with the same energy. In consequence, we consider a biased PAM, in which we design non-negative constellation points belonging to the set $\mathcal{S} = \left\{0, \sqrt{E_{\min}}, 2\sqrt{E_{\min}}, \ldots, (M-1)\sqrt{E_{\min}}\right\}$, where $E_{\min}$ represents the minimum energy difference between adjacent constellation points. Assuming all the symbols are equally likely to be transmitted, the average symbol energy E_{av} is given by [7], [17]

$$E_{\text{av}} = \frac{(M-1)(2M-1)}{6} E_{\min}.$$

Hence, the energy of the m-th symbol is $E_m = m^2 E_{\min}$, for $m = 1, \ldots M$.

Furthermore, at the receiver, the transmitted data from both the activated transmit antenna and the modulation must be detected. Throughout this work, we assume that the detection processes are independent in the calculation[1]. With the focus being on a low-complexity receiver structure, we employ a non-coherent energy detector with knowledge of the fading channel magnitudes [15]. Specifically, the signal is transmitted over an $N_r \times N_t$ wireless channel $\mathbf{H}$, and experiences an N_r-dimensional additive white Gaussian noise (AWGN) vector $\boldsymbol{w} = [w_1 \ldots w_{N_r}]^T$. We assume that the signals from all the receive antennas are combined, and the communication channel is flat Rayleigh fading. Thus, the $N_r N_t$ entries of $\mathbf{H}$ are independent and identically distributed (i.i.d) random variables, each following a complex circular Gaussian random variable with zero mean and variance σ_h^2, i.e., having a

[1]The validity of this assumption lies in the fact that the channel paths are considered uncorrelated, otherwise, the detection processes would be dependent [2].

$\mathcal{CN}(0, \sigma_h^2)$ distribution. In addition, the AWGN vector $\boldsymbol{w}$ follows a $\mathcal{CN}(\mathbf{0}_{N_r}, \sigma_w^2 \mathbf{I}_{N_r})$ distribution, where $\mathbf{0}_{N_r}$ is the $N_r \times 1$ zero-vector, $\mathbf{I}_{N_r}$ is the $N_r \times N_r$ identity matrix, and σ_w^2 is the variance of each element in $\boldsymbol{w}$. We assume a complex baseband signal representation and symbol-by-symbol detection, in which the sampled signal at the i-th receive antenna when s_m is transmitted from the n-th antenna is

$$r_i = h_{i,n} s_m + w_i, \tag{1}$$

where $h_{i,n}$ is the channel coefficient from the n-th transmit antenna to the i-th receive antenna. The symbol s_m has been defined previously and belongs to the constellation set $\mathcal{S}$.

Moreover, the receiver is assumed to have access to the energy of the signal, hence the output of the energy detector at the i-th receive antenna is

$$y_i = |r_i|^2 = |h_{i,n} s_m + w_i|^2. \tag{2}$$

Since the receiver has only knowledge of the magnitudes of the fading gains, i.e., $|h_{i,1}|, \ldots, |h_{i,N_t}|$, then from (2), the observation y_i represents a non-central Chi-squared random variable with two degrees of freedom, non-centrality parameter $|h_{i,n} s_m|^2$, and variance σ_w^2. We define $\beta_{i,n} \triangleq |h_{i,n}|^2$, hence, the conditional probability distribution function (PDF) of y_i conditioned on $\beta_{i,n}$ and E_m, denoted by $f(y_i \mid \beta_{i,n}, E_m)$, is

$$f(y_i \mid \beta_{i,n}, E_m) = \frac{1}{2\sigma_w^2} \exp\left(-\frac{(y_i + \beta_{i,n} E_m)}{2\sigma_w^2}\right) \times I_0\left(\frac{\sqrt{y_i \beta_{i,n} E_m}}{\sigma_w^2}\right), \tag{3}$$

where $I_0(\cdot)$ denotes the modified Bessel function of the zeroth order and the first kind. We observe from (3) that the PDF depends on $\beta_{i,n}$ and E_m. Therefore, it is sufficient to consider only the magnitude of the channel coefficients and non-negative, real-valued symbols.

Given that the receiver is equipped with multiple antennas, and due to the independence of the N_r branches, the joint PDF of the received signal is calculated as the product of the marginal PDFs, i.e., $f(\mathbf{y} \mid \boldsymbol{\beta}_n, E_m) = \prod_{i=1}^{N_r} f(y_i \mid \beta_{i,n}, E_m)$. In order to derive the detection metric, the receiver follows the optimal ML decision rule which jointly searches for $\boldsymbol{\beta}_n$ and E_m that maximizes the natural logarithm of the likelihood function in (3), and is given by [18, Ch. 7, Sec. 7.3]

$$[\hat{n}, \hat{m}] = \arg\max_{n,m} \left[\sum_{i=1}^{N_r} \ln\left\{I_0\left(\frac{2\sqrt{y_i \beta_{i,n} E_m}}{\sigma_w^2}\right)\right\} - \frac{E_m}{\sigma_w^2} \sum_{i=1}^{N_r} \beta_{i,n}\right], \tag{4}$$

where $\hat{n}$ and $\hat{m}$ respectively represent the estimated antenna index and symbol. To apply non-coherent detection to low-complexity receivers, we need to consider a simplification of the optimal decision rule in (4). One such simplification is based on the asymptotic expansion of the Bessel function $I_0(\cdot)$ and its logarithm which is valid at high SNR, by recognizing that $\ln\{I_0(|x|)\} \approx |x|$, for large $|x|$, i.e., high SNR regime. After performing the expansion, the sub-optimal ML decision rule then becomes[2]

$$[\hat{n}, \hat{m}] = \arg\max_{n,m} \left[\sqrt{E_m} \sum_{i=1}^{N_r} \sqrt{y_i \beta_{i,n}} - \frac{E_m}{2} \sum_{i=1}^{N_r} \beta_{i,n}\right]. \tag{5}$$

In the next section, we present an analytical framework to derive closed-form expressions for the SER of the non-coherent SM detector in (5).

III. SER Performance of non-coherent SM

Due to the specific signal structure of SM described in Section II, the transmit vector $\mathbf{x}$ is correctly recovered if both the transmit antenna index and the transmitted symbol are correctly estimated. Hence, it is necessary to split the theoretical analysis into two parts. If we denote by P_{a} the probability that the antenna index estimate is incorrect, and by P_{s} the probability that the transmitted symbol is incorrect, then the overall probability of error, P_{e}, can be written as

$$P_{\mathrm{e}} = P_{\mathrm{a}} + (1 - P_{\mathrm{a}}) P_{\mathrm{s}} = P_{\mathrm{a}} + P_{\mathrm{s}} - P_{\mathrm{a}} P_{\mathrm{s}}. \tag{6}$$

In the next subsections, we deal with the computation of P_{a} and P_{s} separately to compute the overall error probability P_{e}.

A. Analytical SER of P_{s}

Under equiprobable signaling, P_{s} can be expressed as

$$P_{\mathrm{s}} = \frac{1}{M} \sum_{m=0}^{M-1} P_{\mathrm{e}|s_m}, \tag{7}$$

where $P_{\mathrm{e}|s_m}$ is the probability of error when the symbol s_m is transmitted. Since the decision variable $\mathbf{y}$ represents a non-central Chi-square random variable with PDF given in (3), and by employing the decision rule in (5), the probability of detecting E_{m+1} while E_m was transmitted refers to the upper tail of the PDF in (3), which can be characterized by a Chi-square cumulative distribution function (CDF). By symmetry, the probability of detecting E_{m-1} while E_m was transmitted can also be characterized by a Chi-square CDF. Hence, we obtain three cases for $P_{\mathrm{e}|s_m}$ depending on the value of m

$$P_{\mathrm{e}|s_m} = \begin{cases} 1 - F(\rho_m | E_m, \beta), & m = 1 \\ F(\rho_{m-1} | E_m, \beta) + 1 - F(\rho_m | E_m, \beta), & 1 < m < M \\ F(\rho_{m-1} \mid E_m, \beta), & m = M \end{cases}, \tag{8}$$

where $\beta = \sum_{i=1}^{N_r} \beta_i$. $F(\rho_m \mid E_m, \beta)$ is the conditional CDF represented as

$$F(\rho_m \mid E_m, \beta) = 1 - Q_{N_r}\left(\sqrt{\frac{2E_m\beta}{\sigma_w^2}}, \sqrt{\frac{2\rho_m\beta}{\sigma_w^2}}\right),$$

and $Q_{N_r}(\cdot, \cdot)$ is the generalized Marcum Q-function of the N_r-th order, [18, Ch. 4, Sec. 4.2]. The detection threshold ρ_m, $m = 0, 1, \ldots, M-2$, can be approximated as[3]

$$\rho_m \approx \frac{(E_m + E_{m+1})}{2}. \tag{9}$$

[2]The receiver is sub-optimal due to the simplification of the non-linear Bessel function in (4) which makes it applicable to low-complexity receivers [15].

[3]We assume that for high SNR, the PDFs of the decision variables start to resemble a symmetrical distribution, and the thresholds can be bounded by the midpoint of adjacent symbols' energy levels [7].

Ultimately, we can write (7) as

$$P_{\mathrm{s}} = \frac{1}{M}\left[\sum_{m=0}^{M-2} \underbrace{Q_{N_r}\left(\sqrt{\frac{2E_m\beta}{\sigma_w^2}}, \sqrt{\frac{2\rho_m\beta}{\sigma_w^2}}\right)}_{P_1} + \sum_{m=0}^{M-2} \underbrace{1 - Q_{N_r}\left(\sqrt{\frac{2E_{m+1}\beta}{\sigma_w^2}}, \sqrt{\frac{2\rho_m\beta}{\sigma_w^2}}\right)}_{P_2}\right]. \quad (10)$$

It is interesting to note that due to the Marcum Q-function, it is not straightforward to average the SER over the channel magnitude β, hence, we opt to use the following series representation of the generalized Marcum Q-function [19]

$$Q_{N_r}(a,b) = 1 - \exp\left(\frac{-a^2}{2}\right)\sum_{n=0}^{\infty}\left(\frac{a^2}{2}\right)^n \frac{\gamma\left(N_r+n, \frac{b^2}{2}\right)}{\Gamma(N_r+n)}, \quad (11)$$

where $\gamma(\cdot,\cdot)$ is the lower incomplete gamma function, and $\Gamma(\cdot)$ is the Euler (complete) gamma function.

We now start by evaluating P_1 in (10). We apply the following symmetric relation between $Q_{N_r}(a,b)$ and $Q_{N_r}(b,a)$

$$Q_{N_r}(a,b) + Q_{N_r}(b,a) = 1 + e^{-\frac{(a^2+b^2)}{2}} \sum_{k=1-N_r}^{N_r-1}\left(\frac{a}{b}\right)^k I_k(ab), \quad (12)$$

where $I_k(\cdot)$ is the modified Bessel function of the first kind. By using (11) and (12) and after a few algebraic manipulations, we obtain

$$P_1 = \underbrace{\sum_{k=1-N_r}^{N_r-1} \exp\left(-\frac{(E_m+\rho_m)\beta}{\sigma_w^2}\right)\left(\frac{E_m}{\rho_m}\right)^k I_k\left(\frac{2\beta\sqrt{E_m\rho_m}}{\sigma_w^2}\right)}_{P_{11}} + \underbrace{\sum_{n=0}^{\infty}\exp\left(-\frac{\rho_m\beta}{\sigma_w^2}\right)\left(\frac{\rho_m\beta}{\sigma_w^2}\right)^n \frac{\gamma\left(N_r+n, \frac{E_m\beta}{\sigma_w^2}\right)}{\Gamma(N_r+n)}}_{P_{12}}. \quad (13)$$

Each of the P_{11} and P_{12} terms needs to be averaged over the channel magnitudes to obtain the average P_1. For a conditional error function that is non-zero around the origin and that approaches zero with increasing SNR, the SER is dominated by the near-origin behavior of the PDF of the channel gain and characterizes a high SNR performance [20]. Moreover, the Rayleigh distribution of $|h_i|$ leads to an exponential distribution of β_i, and since $\beta = \sum_{i=1}^{N_r}\beta_{i,n} = \sum_{i=1}^{N_r}|h_{i,n}|^2$, then it represents a Gamma distribution with PDF $f_\beta(\beta) = \beta^{N_r-1}\exp(-\beta)/(N_r-1)!$. Thus, the average error rate for P_{11} can be calculated as

$$\begin{aligned}\bar{P}_{11} &= \sum_{k=1-N_r}^{N_r-1}\int_0^\infty \exp\left(-\frac{(E_m+\rho_m)\beta}{\sigma_w^2}\right)\left(\frac{E_m}{\rho_m}\right)^{|k|} \times I_k\left(\frac{2\beta\sqrt{E_m\rho_m}}{\sigma_w^2}\right) f_\beta(\beta)d\beta \\ &= \sum_{k=1-N_r}^{N_r-1}\frac{(|k|+N_r-1)!}{|k|!(N_r-1)!}\left(\frac{E_m}{\rho_m}\right)^{|k|}\left(\frac{E_m\rho_m}{\delta^2}\right)^{\frac{|k|}{2}}\left(\frac{\delta}{\sigma_w^2}\right)^{-N_r} \times {}_2F_1\left(\frac{|k|+N_r}{2}, \frac{|k|+N_r+1}{2}, |k|+1, \frac{4E_m\rho_m}{\delta^2}\right), \end{aligned} \quad (14)$$

where ${}_2F_1(\cdot,\cdot,\cdot,\cdot)$ is the Gaussian hypergeometric function, and we have defined $\delta \triangleq E_m + \rho_m + \sigma_w^2$. Correspondingly, the average error rate for P_{12} is

$$\begin{aligned}\bar{P}_{12} &= \sum_{n=0}^{\infty}\int_0^\infty \exp\left(-\frac{\rho_m\beta}{\sigma_w^2}\right)\left(\frac{\rho_m\beta}{\sigma_w^2}\right)^n \times \frac{\gamma\left(N_r+n, \frac{E_m\beta}{\sigma_w^2}\right)}{\Gamma(N_r+n)} f_\beta(\beta)d\beta \\ &= \sum_{n=0}^{\infty}\frac{(2(n+N_r)-1)!}{(N_r-1)!(n+N_r)!}\left(\frac{\rho_m}{\sigma_w^2}\right)^n\left(\frac{E_m}{\sigma_w^2}\right)^{-n-N_r} \times {}_2F_1\left(n+N_r, 2(n+N_r), n+N_r+1, -\frac{\rho_m+\sigma_w^2}{E_m}\right). \end{aligned} \quad (15)$$

The next step is to evaluate P_2 in (10). We notice by inspection that P_2 can be evaluated similarly as P_{12}. Hence, $\bar{P}_2$ is

$$\begin{aligned}\bar{P}_2 &= \sum_{n=0}^{\infty}\frac{(2(n+N_r)-1)!}{(N_r-1)!(n+N_r)!}\left(\frac{\rho_m}{\sigma_w^2}\right)^{-n-N_r}\left(\frac{E_{m+1}}{\sigma_w^2}\right)^n \\ &\quad \times {}_2F_1\left(n+N_r, 2(n+N_r), n+N_r+1, -\frac{E_{m+1}+\sigma_w^2}{\rho_m}\right). \end{aligned} \quad (16)$$

By substituting (14), (15), and (16) into (10), we obtain a closed-form expression of the average SER for P_{s} in terms of an infinite series.

B. Analytical SER of P_{a} (case $N_t = 2$)

The operation of finding the active transmit antenna is equivalent to solving an N_t-hypothesis testing problem at the receiver. For the sake of analytical simplicity, we first consider the case of $N_t = 2$ and later generalize it to an arbitrary number of transmit antennas. We define $P_{\mathrm{a}}(h_1, h_2)$ as the probability of error of detecting the index of the transmitting antenna

$$P_{\mathrm{a}}(h_1,h_2) = \frac{1}{2}\left[P_{\mathrm{a}}(h_1,h_2)|_{\hat{n}=1} + P_{\mathrm{a}}(h_1,h_2)|_{\hat{n}=2}\right]. \quad (17)$$

Let us start by computing $P_{\mathrm{a}}(h_1,h_2)|_{\hat{n}=1}$. Assuming we know which symbol was transmitted, we denote its energy by E. Furthermore, the channel magnitude is denoted by β_n, for $n = 1, 2$. By referring to (5), we can write

$$P_{\mathrm{a}}(h_1,h_2)=\frac{1}{2}\Bigg[\underbrace{1-Q_{N_r}\left(\frac{\sqrt{E\beta_1}}{\sqrt{\sigma_w^2}},\frac{\sqrt{E\left(\beta_1+\beta_2\right)}}{2\sqrt{\sigma_w^2}}\right)}_{P_3}+\underbrace{Q_{N_r}\left(\frac{\sqrt{E\beta_2}}{\sqrt{\sigma_w^2}},\frac{\sqrt{E\left(\beta_1+\beta_2\right)}}{2\sqrt{\sigma_w^2}}\right)}_{P_4}\Bigg]\cdot\Pr\left\{\beta_1\geq\beta_2\right\}$$
$$+\frac{1}{2}\Bigg[\underbrace{1-Q_{N_r}\left(\frac{\sqrt{E\beta_2}}{\sqrt{\sigma_w^2}},\frac{\sqrt{E\left(\beta_1+\beta_2\right)}}{2\sqrt{\sigma_w^2}}\right)}_{P_5}+\underbrace{Q_{N_r}\left(\frac{\sqrt{E\beta_1}}{\sqrt{\sigma_w^2}},\frac{\sqrt{E\left(\beta_1+\beta_2\right)}}{2\sqrt{\sigma_w^2}}\right)}_{P_6}\Bigg]\cdot\Pr\left\{\beta_1<\beta_2\right\}. \tag{21}$$

$$P_{\mathrm{a}}(h_1,h_2)|_{\hat{n}=1}=\begin{cases}\Pr\left\{|\sqrt{E}r|<\frac{E}{2}(\beta_1+\beta_2)\right\}, \text{ if } \beta_1\geq\beta_2\\ \Pr\left\{|\sqrt{E}r|>\frac{E}{2}(\beta_1+\beta_2)\right\}, \text{ if } \beta_1<\beta_2\end{cases}, \tag{18}$$

where $r=\sum_{i=1}^{N_r} r_i$. Hence, the received signal amplitude $|r|$ can be represented as a Rice distribution with the following CDF

$$F=1-Q_{N_r}\left(\frac{\sqrt{E\beta_1}}{\sqrt{\sigma_w^2}},\frac{\sqrt{E\left(\beta_1+\beta_2\right)}}{2\sqrt{\sigma_w^2}}\right).$$

Therefore, $P_{\mathrm{a}}(h_1,h_2)|_{\hat{n}=1}$ is equivalently written as

$$P_{\mathrm{a}}(h_1,h_2)|_{\hat{n}=1}=\begin{cases}1-Q_{N_r}\left(\frac{\sqrt{E\beta_1}}{\sqrt{\sigma_w^2}},\frac{\sqrt{E(\beta_1+\beta_2)}}{2\sqrt{\sigma_w^2}}\right), \text{if } \beta_1\geq\beta_2\\ Q_{N_r}\left(\frac{\sqrt{E\beta_1}}{\sqrt{\sigma_w^2}},\frac{\sqrt{E(\beta_1+\beta_2)}}{2\sqrt{\sigma_w^2}}\right), \quad \text{if } \beta_1<\beta_2\end{cases}. \tag{19}$$

Following similar steps with $P_{\mathrm{a}}(h_1,h_2)|_{\hat{n}=1}$, we can express $P_{\mathrm{a}}(h_1,h_2)|_{\hat{n}=2}$ as

$$P_{\mathrm{a}}(h_1,h_2)|_{\hat{n}=2}=\begin{cases}1-Q_{N_r}\left(\frac{\sqrt{E\beta_2}}{\sqrt{\sigma_w^2}},\frac{\sqrt{E(\beta_1+\beta_2)}}{2\sqrt{\sigma_w^2}}\right), \text{if } \beta_2\geq\beta_1\\ Q_{N_r}\left(\frac{\sqrt{E\beta_2}}{\sqrt{\sigma_w^2}},\frac{\sqrt{E(\beta_1+\beta_2)}}{2\sqrt{\sigma_w^2}}\right), \quad \text{if } \beta_2<\beta_1\end{cases}. \tag{20}$$

Hence, by combining equations (19) and (20), we can write (18) as given in (21) on top of the page.

As we can see from (21), due to the complexity and intractability of the Marcum Q-function, we follow the same methodology as in the previous section of applying the series representation of the generalized Marcum Q-function in (11). We can also notice from (21) that each error rate expression depends on both channel magnitudes β_1 and β_2. Since we consider the case of i.i.d random variables, the fading channel magnitudes are uncorrelated. In consequence, the joint PDF $f_{\beta_1,\beta_2}(\beta_1,\beta_2)$ can be written as $f_{\beta_1,\beta_2}(\beta_1,\beta_2)=f_{\beta_1}(\beta_1)f_{\beta_2}(\beta_2)$. Thus, we express the average error rate $\bar{P}_3$ as

$$\bar{P}_3=\sum_{n=0}^{\infty}\int_0^{\infty}\int_0^{\beta_1}\exp\left(-\frac{E\beta_1}{2\sigma_w^2}\right)\left(\frac{E\beta_1}{2\sigma_w^2}\right)^n \times\frac{\gamma\left(N_r+n,\frac{E(\beta_1+\beta_2)}{8\sigma_w^2}\right)}{\Gamma\left(N_r+n\right)}f_{\beta_1}(\beta_1)f_{\beta_2}(\beta_2)d\beta_2 d\beta_1. \tag{22}$$

Using (11) and (12), the average error rate $\bar{P}_4$ can be split into two separate expressions, $\bar{P}_{41}$ and $\bar{P}_{42}$, given by

$$\bar{P}_{41}=\sum_{k=1-N_r}^{N_r-1}\int_0^{\infty}\int_0^{\beta_1}\exp\left(-\frac{E(\beta_1+5\beta_2)}{8\sigma_w^2}\right)\left(\frac{4\beta_2}{\beta_1+\beta_2}\right)^{\frac{|k|}{2}} \times I_k\left(\frac{E\sqrt{\beta_2(\beta_1+\beta_2)}}{2\sigma_w^2}\right)f_{\beta_1}(\beta_1)f_{\beta_2}(\beta_2)d\beta_2 d\beta_1. \tag{23}$$

$$\bar{P}_{42}=\sum_{n=0}^{\infty}\int_0^{\infty}\int_0^{\beta_1}\exp\left(-\frac{E\left(\beta_1+\beta_2\right)}{8\sigma_w^2}\right)\left(\frac{E\left(\beta_1+\beta_2\right)}{8\sigma_w^2}\right)^n \times\frac{\gamma\left(N_r+n,\frac{E\beta_2}{2\sigma_w^2}\right)}{\Gamma(N_r+n)}f_{\beta_1}(\beta_1)f_{\beta_2}(\beta_2)d\beta_2 d\beta_1. \tag{24}$$

Due to the symmetry of the problem and space limitations, the error rate expressions P_5 and P_6 in (21) can be solved in the same manner as P_3 and P_4, respectively, by inverting the order of the integrals. Ultimately, by substituting (10) and (21) in (6), we obtain the expression for the overall error probability for non-coherent SM.

C. Generalization to an $N_t \times N_r$ SM System

In this subsection, we provide a generalization to the analysis presented earlier, where we saw the case of a $2 \times N_r$ system. Due to the noticeable analytical complexity for the case where $N_t = 2$, we express the generalized case based on the result obtained previously. Specifically, the generalized antenna index error rate can be expressed as

$$P_{\mathrm{a}}^{\mathrm{G}}=\frac{1}{2(N_t-1)}\sum_{t=1}^{N_t}\sum_{t'=t+1}^{N_t}P_{\mathrm{a}}\left(h_t,h_{t'}\right). \tag{25}$$

Here, $P_{\mathrm{a}}\left(h_t,h_{t'}\right)$ is similar to $P_{\mathrm{a}}(h_1,h_2)$ in (21) when transmit antenna 1 and 2 are considered. The rest of the transmit antennas are tested by combining t and t' for all possible pairs.

IV. Simulation Results

In this section, we present numerical results of the proposed energy detector for non-coherent SM. In the simulations, we consider a flat Rayleigh fading channel with AWGN and channel magnitude knowledge at the receiver. We consider two schemes as benchmarks for performance; C-ML is the SM optimal (coherent) ML receiver [11], where $\beta_{i,n}$ is replaced by $h_{i,n}^2$ in (5), and MRC is the SM MRC receiver in [2].

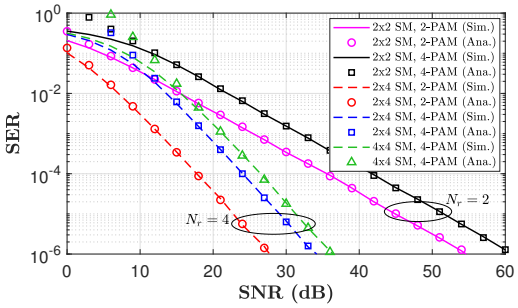

Fig. 2: Validation of theoretical analysis for different combinations of system parameters N_t, N_r, and M.

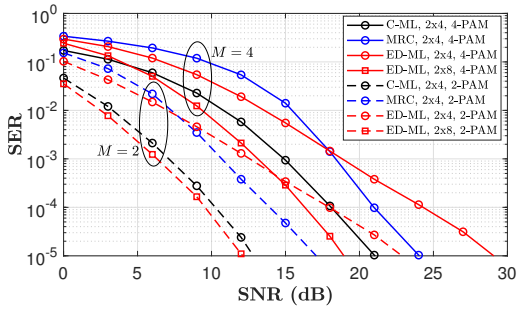

Fig. 3: Performance of ED-ML versus C-ML and MRC for 2 and 4-level biased PAM ($M = 2, 4$).

The proposed receiver is denoted by ED-ML. Ultimately, we evaluate the performance in terms of the SER versus the SNR.

We first validate our theoretical SER analysis in Fig. 2 where we show the performance of the proposed ED-ML receiver for $N_t = 2$, $N_r = 2, 4$, and $M = 2, 4$. The results show that there is a perfect match between the numerical and the analytical/theoretical SER for various cases.

We then compare the performance of ED-ML with that of C-ML and MRC for two-level and four-level biased PAM in Fig. 3. We perceive that with the increase in modulation order, non-coherent detection outperforms its coherent counterpart. For instance, at an error rate of 10^{-5}, the gap between 2-PAM (dashed lines) and 4-PAM (solid lines) is around 9 dB for C-ML, 7.5 dB for MRC, and 6 dB for ED-ML. This result highlights the importance of employing a non-negative constellation design which is only optimal for the case of non-coherent reception. In addition, we plot the performance of the ED-ML scheme for the case where the receiver is equipped with $N_r = 8$ antennas (square markers). We observe that in order to outperform the C-ML for the same modulation order, the receiver must be equipped with more antennas (four more antennas in this case) to compensate for the fact of having partial channel knowledge.

V. Conclusion

In this paper, we presented a non-coherent spatial modulation detection scheme based on the maximum likelihood criterion, with channel magnitude knowledge at the receiver. We analyzed the performance of our design by computing the average SER at high SNRs when employing a biased (non-negative) PAM. Our results showed that the performance of non-coherent SM is superior to that of its coherent counterpart when employing non-negative constellations. Due to its low complexity and partial channel knowledge, an important application for non-coherent SM is for low-cost low-powered IoT devices.

References

[1] A. Al-Fuqaha, M. Guizani, M. Mohammadi, M. Aledhari, and M. Ayyash, "Internet of Things: A survey on enabling technologies, protocols, and applications," *IEEE Commun. Surv. Tuts.*, vol. 17, no. 4, pp. 2347–2376, 2015.

[2] R. Y. Mesleh, H. Haas, S. Sinanovic, C. W. Ahn, and S. Yun, "Spatial modulation," *IEEE Trans. Veh. Technol.*, vol. 57, no. 4, pp. 2228–2241, Jul. 2008.

[3] R. Mesleh, H. Haas, C. W. Ahn, and S. Yun, "Spatial modulation - A new low complexity spectral efficiency enhancing technique," in *Proc. IEEE Int. Conf. Commun. Netw. China*, Beijing, China, Oct. 2006, pp. 1–5.

[4] A. Stavridis, S. Sinanovic, M. Di Renzo, and H. Haas, "Energy evaluation of spatial modulation at a multi-antenna base station," in *Proc. 78th IEEE Veh. Technol. Conf. (VTC)*, Las Vegas, NV, USA, Sep. 2013, pp. 1–5.

[5] D. Feng, C. Jiang, G. Lim, L. J. Cimini, G. Feng, and G. Y. Li, "A survey of energy-efficient wireless communications," *IEEE Commun. Surv. Tuts.*, vol. 15, no. 1, pp. 167–178, First Quarter 2013.

[6] X.-C. Gao, J.-K. Zhang, H. Chen, Z. Dong, and B. Vucetic, "Energy-efficient and low-latency massive SIMO using noncoherent ML detection for industrial IoT communications," *IEEE Internet Things J.*, vol. 6, no. 4, pp. 6247–6261, Aug. 2019.

[7] A. Anttonen, A. Mammela, and A. Kotelba, "Error probability of energy detected multilevel PAM signals in lognormal multipath fading channels," in *IEEE Int. Conf. Commun.* Dresden, Germany: IEEE, Jun. 2009, pp. 1–5.

[8] S.-K. Yong, P. Xia, and A. Valdes-Garcia, *60GHz Technology for Gbps WLAN and WPAN: from Theory to Practice*. John Wiley & Sons, 2011.

[9] X. Zhou, R. Zhang, and C. K. Ho, "Wireless information and power transfer: Architecture design and rate-energy tradeoff," *IEEE Trans. Commun.*, vol. 61, no. 11, pp. 4754–4767, Nov. 2013.

[10] J. J. Park, J. H. Moon, K.-Y. Lee, and D. I. Kim, "Transmitter-oriented dual-mode SWIPT with deep-learning-based adaptive mode switching for IoT sensor networks," *IEEE Internet Things J.*, vol. 7, no. 9, pp. 8979–8992, Sep. 2020.

[11] J. Jeganathan, A. Ghrayeb, and L. Szczecinski, "Spatial modulation: Optimal detection and performance analysis," *IEEE Commun. Lett.*, vol. 12, no. 8, pp. 545–547, 2008 2008.

[12] A. Younis, M. Di Renzo, R. Mesleh, and H. Haas, "Sphere decoding for spatial modulation," in *Proc. IEEE Int. Conf. Commun. (ICC)*. Kyoto, Japan: IEEE, Jun. 2011, pp. 1–6.

[13] M. Maleki, H. R. Bahrami, and A. Alizadeh, "On MRC-based detection of spatial modulation," *IEEE Trans. Wireless Commun.*, vol. 15, no. 4, pp. 3019–3029, Apr. 2016.

[14] J. Wang, S. Jia, and J. Song, "Signal vector based detection scheme for spatial modulation," *IEEE Commun. Lett.*, vol. 16, no. 1, pp. 19–21, Jan. 2012.

[15] R. K. Mallik, R. D. Murch, and Y. Li, "Channel magnitude based energy detection with receive diversity for multi-level amplitude-shift keying in rayleigh fading," *IEEE Trans. Commun.*, vol. 65, no. 7, pp. 3079–3094, Jul. 2017.

[16] M. Di Renzo and H. Haas, "Space shift keying (SSK) modulation with partial channel state information: Optimal detector and performance analysis over fading channels," *IEEE Trans. Commun.*, vol. 58, no. 11, pp. 3196–3210, Nov. 2010.

[17] M. Secondini and E. Forestieri, "Direct detection of bipolar pulse amplitude modulation," *J. Lightw. Technol.*, vol. 38, no. 21, pp. 5981–5990, Jul. 2020.

[18] M. K. Simon and M.-S. Alouini, *Digital communication over fading channels*. John Wiley & Sons, 2005, vol. 95.

[19] N. Temme, "Asymptotic and numerical aspects of the noncentral Chi-square distribution," *Comput. Math. Appl.*, vol. 25, no. 5, pp. 55–63, 1993.

[20] Z. Wang and G. B. Giannakis, "A simple and general parameterization quantifying performance in fading channels," *IEEE Trans. Commun.*, vol. 51, no. 8, pp. 1389–1398, Aug. 2003.